Inorganic Composites

DOI: 10.1002/anie.200906642

Modular Inorganic Nanocomposites by Conversion of Nanocrystal Superlattices**

*Ravisubhash Tangirala, Jessy L. Baker, A. Paul Alivisatos, and Delia J. Milliron**

Inorganic nanocomposites have recently emerged as a means of controlling material functionality by morphology and composition to give combinations of properties not generally found in homogeneous single-phase materials. For example, battery electrodes must efficiently conduct both electrons and ions to achieve high power,[1] whereas thermoelectric energy conversion is most efficient when electrical conductivity is high yet thermal conductivity is low.[2] However, the development of nanocomposites for such applications is hindered by the lack of a general fabrication method capable of controlling morphology over a wide range of compositions. Recently, exquisite control over colloidal nanocrystal assembly has been developed, including highly ordered superlattices,[3] binary nanocrystal assemblies,[4] and oriented nanorod assemblies.[5] Herein we show that such nanocrystal assemblies can be converted into inorganic nanocomposites by the post-assembly replacement of organic ligands with inorganic chalcogenidometallate clusters (ChaMs). The nanocrystals and ChaMs[6] are synthesized and processed independently, so this approach affords complete compositional modularity. Critically, the morphology of the original nanocrystal assemblies, including oriented nanorod assemblies, is maintained in the resulting nanocomposites.

[*] Dr. R. Tangirala, Dr. D. J. Milliron
The Molecular Foundry, Lawrence Berkeley National Laboratory
1 Cyclotron Road, Berkeley, CA 94720 (USA)
Fax: (+1) 510-486-6166
E-mail: dmilliron@lbl.gov
Homepage: http://foundry.lbl.gov/six/inorganic/staff-Delia_Milliron.html

J. L. Baker
Departments of Mechanical Engineering and Chemistry
University of California, Berkeley
Berkeley, CA 94720 (USA)

Prof. A. P. Alivisatos
Department of Chemistry, University of California, Berkeley
and
Materials Sciences Division, Lawrence Berkeley National Laboratory
Berkeley, CA 94720 (USA)

[**] We gratefully acknowledge D. K. Ko for providing PbSe nanocrystals, S. Aloni for assistance with TEM imaging, A. Hexemer for assistance and guidance with GISAXS measurements, and R. Y. Wang and J. J. Urban for several helpful discussions. J.L.B. was supported by a doctoral fellowship from the National Science Foundation. This work was supported in part by the Laboratory Directed Research and Development Program of Lawrence Berkeley National Laboratory and work was completed at the Molecular Foundry, support by the Office of Science, Office of Basic Energy Sciences, of the U.S. Department of Energy under contract no. DE-AC02-05CH11231.

Supporting information for this article is available on the WWW under http://dx.doi.org/10.1002/anie.200906642.

Compelled by the unique properties achievable in inorganic nanocomposites, several approaches to their fabrication have been shown for specific applications. For example, spinodal decomposition and precipitation of a secondary phase of PbS within a PbTe matrix was used to generate a nanostructured thermoelectric composite.[2b] Whilst remarkable improvements in thermoelectric efficiency resulted, the ability to tune morphological characteristics such as the size of the nanoinclusions is limited, and the achievable compositions are severely restricted. A more general approach, which has been applied to battery electrodes, is to mechanically mill the component materials until they intermix on the nanoscale.[1b] The cost of generality, however, is a failure to reliably create intimate contact between the components, and morphology is again poorly controlled. Another elegant example is the co-assembly of solution-processed building blocks into ordered arrays of gold nanoparticles within a silica matrix, which provides thermal stability.[7] However, this method cannot be applied to arbitrary compositions as it relies on the carefully balanced interaction of the two components, together with a structure-directing surfactant, under dynamic solvent evaporation conditions. In a recent report, solution-phase ligand exchange in a strongly reducing environment was used to adsorb ChaMs to the surfaces of solvent-dispersed nanocrystals.[8] These ChaM-coated nanocrystals could then be deposited to form composite films, although the harsh conditions limit the compositional applicability, and general approaches to assemble the resulting charged nanocrystals are lacking. Underscoring these limitations, in only one case, namely gold nanoparticles with Sn-S ligands, was preparation of an ordered assembly demonstrated, and no evidence for ordering on a large scale was reported.

In contrast, our approach uses methods for assembling nanocrystals terminated by organic ligands; these methods have been refined for over a decade. For example, vertically oriented arrays of semiconductor nanorods have been prepared by controlled evaporation,[5a,9] electric field orientation,[5b,c] or evaporation at the air–water interface,[5d] all of which depend on the organic ligand coating to mediate nanorod interactions with each other and their environment. Similarly, control over binary nanocrystal assemblies was found to depend critically on the presence of ligands.[4a] Recently, electronic applications of nanocrystal assemblies have gained momentum because it was demonstrated that their conductivity can be greatly enhanced by post-assembly replacement of bulky organic ligands with much smaller molecules, such as hydrazine[10a] or ethylenediamine.[10b] This process takes full advantage of nanocrystal assembly techniques so that, for example, heterogeneous doping could be

observed in binary assemblies of Ag_2Te and PbTe nanocrystals.[2a] However, the electronic properties of such materials are strongly history-dependent owing to the reactivity and volatility of the small molecules employed.[10a] Nonetheless, these exchange processes are highly versatile and applicable to nanocrystal assemblies of all types.

Inspired by this approach, we now report the fabrication of purely inorganic nanocomposites by post-assembly conversion of nanocrystal superlattices, which allows modular selection of composition for targeted electronic applications. For example, PbSe nanocrystals, ideal for transistors[10a] and thermoelectric applications,[2] form close-packed hexagonal assemblies in which the particle spacing is initially dictated by the oleic acid ligand coating (Figure 1 a,c). To convert the

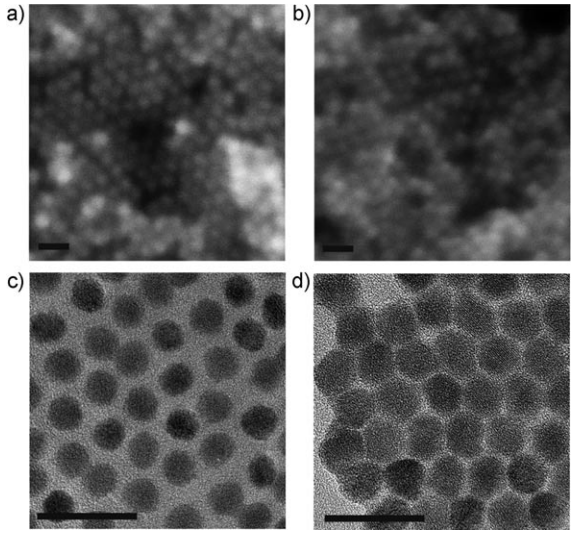

Figure 1. Formation of a PbSe-Sb_2Se_3 nanocomposite from a PbSe nanocrystal superlattice. a,b) SEM images of a PbSe nanocrystal film: a) the original superlattice, and b) after ligand exchange with an Sb-Se ChaM; c,d) TEM images of c) a PbSe nanocrystal superlattice, and d) PbSe-Sb_2Se_3 nanocomposite film. Scale bars: 20 nm.

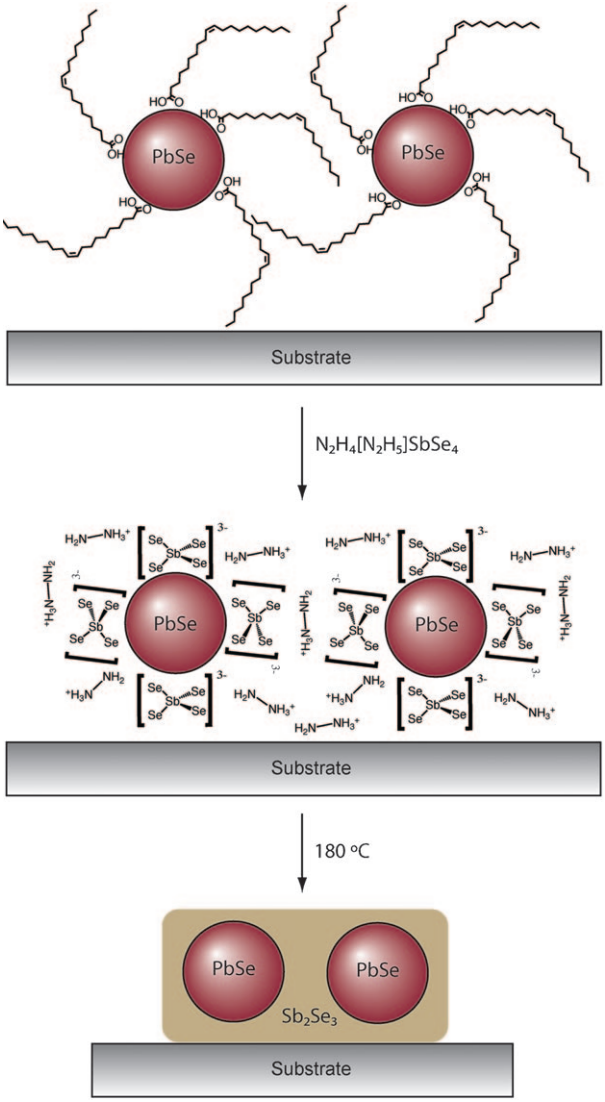

Scheme 1. Representation of the fabrication of a PbSe-Sb_2Se_3 nanocomposite by post-assembly replacement of oleic acid ligands with an Sb-Se ChaM and subsequent annealing at 180 °C.

superlattice into an inorganic nanocomposite, we immersed it in a ChaM solution and allowed the clusters to displace the organic ligands by mass action (Scheme 1). Targeting a composition of interest for thermoelectrics, PbSe superlattices were soaked in an Sb-Se ChaM solution, then rinsed to remove any superficial Sb-Se. Following this process, the nanocrystal superlattices are intact and still readily observable by high resolution scanning electron microscopy (HRSEM; Figure 1 b), but now the composition of the assembly, measured by energy dispersive X-ray spectroscopy (EDS), includes 8–14 % Sb and less than 5 % C. To illustrate the generality of this procedure, 20 different combinations of materials have been incorporated into nanocomposites to date in this way (Supporting Information, Figures S1,2). The ChaM can be cross-linked by thermal annealing, eliminating hydrazinium cations and excess chalcogen to give a pure metal chalcogenide secondary phase. Elemental mapping reveals a uniform composition with no evidence of phase segregation (Supporting Information, Figure S3).

Following conversion into a nanocomposite, the TEM contrast between the PbSe nanocrystals and the inter-particle material is substantially reduced, which is consistent with the replacement of the organic ligands with inorganic material (Figure 1 d; Supporting Information, Figure S2). Furthermore, although the hexagonal ordering of the nanocrystals is largely maintained, the center-to-center distance decreases from about 10.5 nm to about 8 nm. The recent report by Talapin et al.[8] demonstrates that ChaMs associate with nanocrystal surfaces; we suggest that this cluster–surface interaction facilitates the post-assembly conversion process, resulting in reduced particle spacing similar to that observed when bulky ligands are displaced by small organic molecules.[10a,b] As in that case, volume contraction during conversion induces cracks, which can be filled in subsequent deposition steps to create a continuous nanocomposite film. This cracking could be minimized by replacing the ligands with

shorter-chain ligands, such as butyl groups, prior to assembly.[10c]

Although electron microscopy establishes that local order is maintained in the conversion from a nanocrystal superlattice into an inorganic nanocomposite, an ensemble approach is needed to evaluate the overall morphology changes induced by the process. To that end, grazing-incidence small-angle X-ray scattering (GISAXS) patterns were recorded, averaging information from a circa 0.5 × 25 mm region of the sample. The initial PbSe superlattice has a highly textured scattering pattern (Figure 2a), indicating excellent in-plane and vertical packing and hexagonal ordering. The texture observed is similar to that previously reported for a PbSe nanocrystal film[10a] and is consistent with randomly oriented superlattice domains. Following ligand displacement by the Ge-S ChaM, the three-dimensional ordering is initially disturbed, as seen by isotropic scattering (Figure 2b). After annealing, however, the ordering largely recovers (Figure 2c). The presence of reflections in the two-dimensional plane suggests three-dimensional ordering, similar to the original assembly. Reduced scattering intensity is consistent with lower contrast, owing to an all-inorganic composition. Similar results were observed for PbSe-Sb_2Se_3 nanocomposites; the GISAXS pattern of this material implies regular interparticle spacing but reduced three-dimensional ordering (Supporting Information, Figure S4). Linecuts along the q_y (horizontal) axis of the GISAXS patterns reveal a decrease in the average in-plane center-to-center distance (Figure 2d; Supporting Information, Figure S4) from 10.1 nm in the original assembly to 7.6 nm in the PbSe-Sb_2Se_3 composite, and 7.7 nm in the PbSe-GeS_2 composite, which is consistent with the TEM observations.

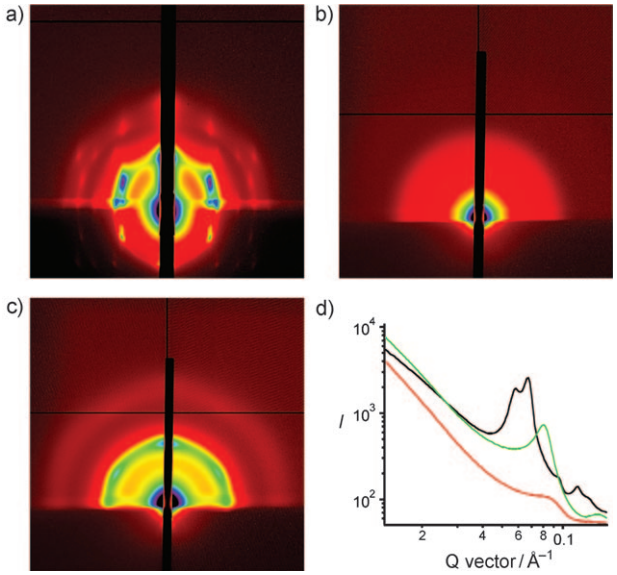

Figure 2. a–c) Two-dimensional GISAXS patterns obtained from: a) the PbSe nanocrystal superlattice, b) PbSe film soaked in Ge-S ChaM solution, and c) PbSe-GeS_2 nanocomposite film after annealing. d) $I(q)$ versus q plots obtained by taking linecuts of the GISAXS data along the horizontal (q_y) axis. Peaks correspond to center-to-center spacing. Traces refer to the original PbSe superlattice (black), PbSe-Ge-S ChaM film (red), and annealed PbSe-GeS_2 nanocomposite (green).

Although composites based on close-packed spheres are attractive for thermoelectrics, a vertically oriented nanorod composite is ideal for efficient photoinduced charge separation and collection.[11a] Heterojunctions of CdS with Cu_2S are of renewed interest for photovoltaic cells,[11b] so we investigated the conversion of vertically oriented assemblies of CdS nanorods, prepared by controlled evaporation,[9] into a nanocomposite by employing a Cu-S ChaM ($(Cu_7S_4)^{-1}$).[6b,e] As seen by TEM, the initial nanorod assembly contains vertically aligned regions surrounded by inclined nanorods with hexagonal ordering (Figure 3a). This observation is confirmed by GISAXS, in which the near-vertical orientation of the nanorods is shown by truncated, slightly curved Bragg rods (Supporting Information, Figure S5a). The aligned nanorod arrays were converted into a nanocomposite by soaking in a Cu-S ChaM solution, followed by annealing at 180 °C. TEM of the resulting composite confirms that the nanorods retain much of the original vertical orientation, similarly exhibiting small areas of vertically aligned nanorods surrounded by tilted nanorods (Figure 3b). The nanocomposite contains 8–10 % Cu and the TEM contrast between the nanorods and the inter-particle phase is dramatically reduced, similar to the nanosphere composites. A GISAXS pattern of the nanocomposite contains reflections on the q_y axis corresponding to the regular center-to-center spacing of the nanorods (Supporting Information, Figure S5b). These truncated Bragg rods, and the absence of a ring arising from isotropic nanorod orientation, confirm that vertical orientation is largely retained. The shrinkage of the Bragg rods may be caused by deterioration of in-plane ordering and also a decrease in the X-ray scattering contrast.

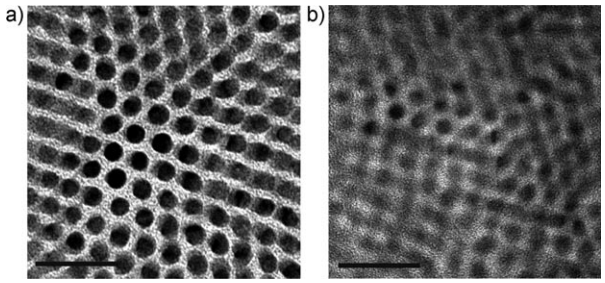

Figure 3. Fabrication of CdS-Cu_2S nanocomposites from CdS nanorod arrays. TEM images of a) the original nanorod array, and b) CdS-Cu_2S composite made from the nanorod array. Scale bars: 20 nm.

Along with their potential application as electronic materials, such as in transistors, photovoltaic cells, and thermoelectric devices, inorganic nanocomposites can also facilitate the investigation of temperature-dependent properties of nanomaterials. The thermal stability of our PbSe-based nanocomposites was established by X-ray diffraction (XRD; Figure 4a). Using the Scherrer equation to calculate crystallite size from the width of the (200) reflection, we find that the original nanocrystal size of 7 nm is approximately maintained in the thermally annealed composites (6.6 nm). In contrast, a

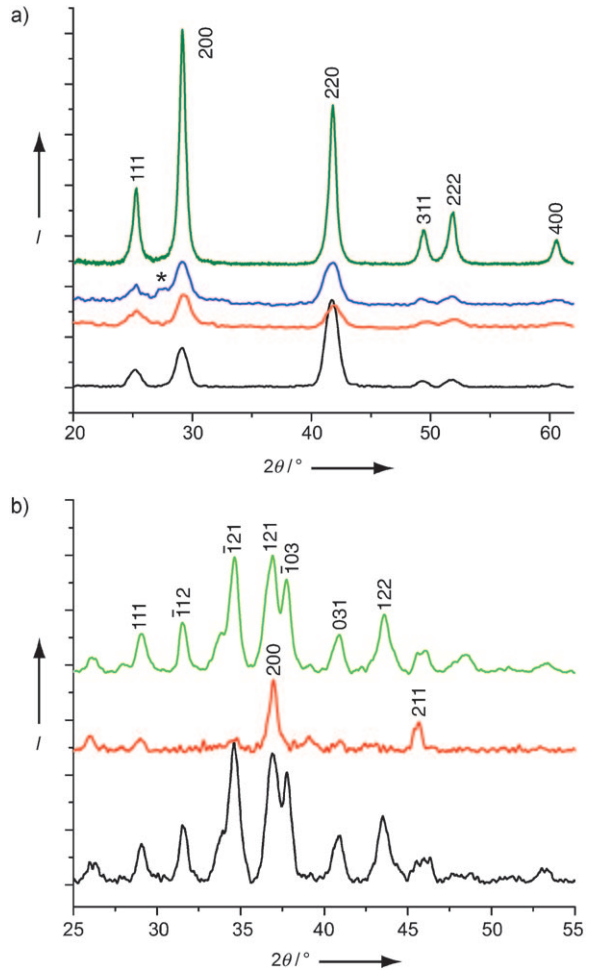

Figure 4. X-ray diffraction of nanocomposites. a) The initial PbSe nanocrystals (black) sinter upon heating (green), whereas the small crystal size is maintained in composites with Sb_2Se_3 (blue) and GeS_2 (red) matrices. Only the strongest, broad peak is visible from orthorhombic Sb_2Se_3 in the PbSe-Sb_2Se_3 composite (⋆). Peaks were assigned according to JCPDS files 01-078-1903 for PbSe and 00-015-0861 for Sb_2Se_3. b) Ag_2S nanocrystals in a Ag_2S-GeS_2 nanocomposite undergo a superionic phase transition from monoclinic at room temperature (black) to cubic at 250 °C (red) and back upon cooling (green) without sintering. Peaks were assigned according to JCPDS files 00-014-0072 (monoclinic) and 01-076-0134 (cubic) Ag_2S.

film of organic ligand-capped PbSe nanocrystals annealed at 200 °C sinters significantly, resulting in 14 nm crystallites. We conclude that the presence of the inorganic matrix around the nanocrystals protects them from sintering. This characteristic facilitates the study of size-dependent properties because particle size can be maintained during thermal cycling. For example, Ag_2S nanocrystals, contained within a GeS_2 matrix, could be cycled to 250 °C through a phase transition to the superionic cubic phase and back again without sintering (Figure 4b). For circa 10 nm particles of AgI, it has been shown that hysteresis of the analogous phase transition stabilizes the superionic phase at room temperature.[12] Therefore, we suggest that incorporating electrochemically active nanoparticles into composites by our modular methodology is a way to exploit such size effects in next-generation battery electrodes.

In summary, we have demonstrated a general route to fabricate modular inorganic nanocomposites by conversion of nanocrystal assemblies, including vertically aligned nanorod arrays. Decoupling the assembly and composite forming steps enables morphological and compositional control to be achieved. The methods outlined herein greatly enhance flexibility for systematic exploration and optimization of nanocomposite properties, and enable development of materials for an open-ended list of applications that could benefit from well-controlled chemically and morphologically tunable all-inorganic nanocomposites.

Experimental Section

PbSe nanocrystals with average size of (7 ± 0.4) nm and first absorption feature at 2165 nm were synthesized using a modified literature procedure from PbO and TOP-Se.[13] CdS nanorods (ca. (4 ± 0.4) nm in diameter and (35 ± 4) nm in length) were synthesized by a literature procedure from CdO and TOP-S.[14] Ag_2S nanocrystals (ca. 8 nm in diameter) were synthesized by the sulfidation of Ag nanocrystals by a modified literature procedure.[15] Details of all the synthetic procedures are provided in the Supporting Information.

ChaMs were prepared at room temperature in a nitrogen-atmosphere glovebox by dissolution of metal chalcogenides in distilled anhydrous hydrazine in the presence of excess chalcogen. *Caution!* Hydrazine is highly toxic and should be handled with extreme caution to prevent exposure by inhalation or absorption through the skin. The Ge-S ChaM is analogous to a previously reported Ge-Se ChaM,[6d] and is expected to have the chemical formula $(N_2H_4)_x(N_2H_5)_4Ge_2S_6$. For ligand exchange, solutions of the ChaMs were prepared at concentrations of 10–67 mg mL^{-1}.

Nanocomposite preparation was performed in a nitrogen-atmosphere glovebox. PbSe or Ag_2S nanocrystal films were first deposited from hexane–octane dispersions. Vertically oriented CdS nanorod arrays were formed by controlled evaporation.[9] Nanocrystal films were then placed in ChaM solutions for 20–40 min to carry out the ligand exchange. The samples were then rinsed to remove excess ChaM and any remaining organic ligand, followed by thermal decomposition of the ChaM. GISAXS measurements were performed at beamline 7.3.3 at the Advanced Light Source, Lawrence Berkeley National Laboratory, using a circa 0.5 mm wide 10 keV X-ray beam.

Received: November 25, 2009
Published online: March 18, 2010

Keywords: composites · ligand exchange · nanostructures · self-assembly · solution processing

[1] a) P. G. Bruce, B. Scrosati, J. M. Tarascon, *Angew. Chem.* **2008**, *120*, 2972; *Angew. Chem. Int. Ed.* **2008**, *47*, 2930; b) F. Badway, N. Pereira, F. Cosandey, G. G. Amatucci, *J. Electrochem. Soc.* **2003**, *150*, A1209; c) B. Kang, G. Ceder, *Nature* **2009**, *458*, 190.
[2] a) J. J. Urban, D. V. Talapin, E. V. Shevchenko, C. R. Kagan, C. B. Murray, *Nat. Mater.* **2007**, *6*, 115; b) J. Androulakis, C. H. Lin, H. J. Kong, C. Uher, C. I. Wu, T. Hogan, B. A. Cook, T. Caillat, K. M. Paraskevopoulos, M. G. Kanatzidis, *J. Am. Chem. Soc.* **2007**, *129*, 9780.
[3] M. P. Pileni, *J. Phys. Chem. B* **2001**, *105*, 3358.
[4] a) E. V. Shevchenko, D. V. Talapin, N. A. Kotov, S. O'Brien, C. B. Murray, *Nature* **2006**, *439*, 55; b) D. K. Smith, B. Good-

fellow, D. M. Smilgies, B. A. Korgel, *J. Am. Chem. Soc.* **2009**, *131*, 3281.
[5] a) P. D. Cozzoli, T. Pellegrino, L. Manna, *Chem. Soc. Rev.* **2006**, *35*, 1195; b) K. M. Ryan, A. Mastroianni, K. A. Stancil, H. T. Liu, A. P. Alivisatos, *Nano Lett.* **2006**, *6*, 1479; c) S. Gupta, Q. L. Zhang, T. Emrick, T. P. Russell, *Nano Lett.* **2006**, *6*, 2066; d) J. He, Q. Zhang, S. Gupta, T. Emrick, T. R. Russell, P. Thiyagarajan, *Small* **2007**, *3*, 1214; e) N. R. Jana, *Angew. Chem.* **2004**, *116*, 1562; *Angew. Chem. Int. Ed.* **2004**, *43*, 1536.
[6] a) E. Ruzin, E. Zent, E. Matern, W. Massa, S. Dehnen, *Chem. Eur. J.* **2009**, *15*, 5230; b) D. J. Milliron, D. B. Mitzi, M. Copel, C. E. Murray, *Chem. Mater.* **2006**, *18*, 587; c) D. J. Milliron, S. Raoux, R. Shelby, J. Jordan-Sweet, *Nat. Mater.* **2007**, *6*, 352; d) D. B. Mitzi, *Inorg. Chem.* **2005**, *44*, 3755; e) D. B. Mitzi, *Inorg. Chem.* **2007**, *46*, 926; f) D. B. Mitzi, L. L. Kosbar, C. E. Murray, M. Copel, A. Afzali, *Nature* **2004**, *428*, 299.
[7] H. Y. Fan, K. Yang, D. M. Boye, T. Sigmon, K. J. Malloy, H. F. Xu, G. P. Lopez, C. J. Brinker, *Science* **2004**, *304*, 567.
[8] M. V. Kovalenko, M. Scheele, D. V. Talapin, *Science* **2009**, *324*, 1417.
[9] J. L. Baker, A. Widmer-Cooper, M. Toney, P. Geissler, A. P. Alivisatos, *Nano Lett.* **2010**, *10*, 195.
[10] a) D. V. Talapin, C. B. Murray, *Science* **2005**, *310*, 86; b) J. E. Murphy, M. C. Beard, A. J. Nozik, *J. Phys. Chem. B* **2006**, *110*, 25455; c) E. J. D. Klem, D. D. MacNeil, P. W. Cyr, L. Levina, E. H. Sargent, *Appl. Phys. Lett.* **2007**, *90*, 183113.
[11] a) W. U. Huynh, J. J. Dittmer, A. P. Alivisatos, *Science* **2002**, *295*, 2425; b) Y. Wu, C. Wadia, W. L. Ma, B. Sadtler, A. P. Alivisatos, *Nano Lett.* **2008**, *8*, 2551.
[12] R. Makiura, T. Yonemura, T. Yamada, M. Yamauchi, R. Ikeda, H. Kitagawa, K. Kato, M. Takata, *Nat. Mater.* **2009**, *8*, 476.
[13] a) J. S. Steckel, B. K. H. Yen, D. C. Oertel, M. G. Bawendi, *J. Am. Chem. Soc.* **2006**, *128*, 13032; b) W. W. Yu, J. C. Falkner, B. S. Shih, V. L. Colvin, *Chem. Mater.* **2004**, *16*, 3318.
[14] Z. A. Peng, X. G. Peng, *J. Am. Chem. Soc.* **2001**, *123*, 183.
[15] D. S. Wang, T. Xie, Q. Peng, Y. D. Li, *J. Am. Chem. Soc.* **2008**, *130*, 4016.

